

Article

Research of Structural, Strength and Thermal Properties of ZrO₂—CeO₂ Ceramics Doped with Yttrium

Sholpan G. Giniyatova¹, Nurzhan A. Sailaukhanov¹, Eugeny Nesterov², Maxim V. Zdorovets^{1,3,4} , Artem L. Kozlovskiy^{3,5}  and Dmitriy I. Shlimas^{1,3,*}

¹ Engineering Profile Laboratory, L.N. Gumilyov Eurasian National University, Nur-Sultan 010008, Kazakhstan; giniyatova_shg@enu.kz (S.G.G.); nsailaukhanov@gmail.com (N.A.S.); mzdorovets@inp.kz (M.V.Z.)

² Educational and Scientific Center “Research Nuclear Reactor” of the School of Nuclear Technology Engineering, Tomsk Polytechnic University, 634050 Tomsk, Russia; nea@tpu.ru

³ Laboratory of Solid State Physics, The Institute of Nuclear Physics, Almaty 050032, Kazakhstan; kozlovskiy.a@inp.kz

⁴ Department of Intelligent Information Technologies, Ural Federal University, 620075 Yekaterinburg, Russia

⁵ Institute of Geology and Oil and Gas Business, Satbayev University, Almaty 050032, Kazakhstan

* Correspondence: shlimas@mail.ru

Abstract: In this work, using a mechanochemical solid-phase synthesis method, ZrO₂—CeO₂ ceramics doped with yttrium were obtained, which have great prospects for use as a basis for dispersed nuclear fuel materials or inert nuclear fuel matrices. The purpose of this work was to study the formation of the ZrO₂—CeO₂ phase composition, depending on the concentration of yttrium dopant, as well as to study their structural and strength properties. The relevance of this study is in obtaining new data on the properties of composite ceramics based on oxides having a cermet structure, as well as the effect of doping with yttrium on increasing the resistance of ceramics to deformation and thermal properties. During the studies, the dynamics of the phase transformations depending on the concentration of the dopant, as well as changes in the structural characteristics and dislocation density, were established. It was found that at a dopant concentration of 0.25 mol, the main phase in the structure was Ce₃ZrO₈—triclinic *P1* (1), the formation of which led to an increase in the mechanical and strength properties of the ceramics as well as a 1.5-fold increase in the thermal conductivity coefficient.

Keywords: oxide ceramics; inert matrices; phase transformations; doping; zirconium dioxide



Citation: Giniyatova, S.G.; Sailaukhanov, N.A.; Nesterov, E.; Zdorovets, M.V.; Kozlovskiy, A.L.; Shlimas, D.I. Research of Structural, Strength and Thermal Properties of ZrO₂—CeO₂ Ceramics Doped with Yttrium. *Crystals* **2022**, *12*, 242. <https://doi.org/10.3390/cryst12020242>

Academic Editor: Maria Gazda

Received: 31 January 2022

Accepted: 8 February 2022

Published: 10 February 2022

Publisher's Note: MDPI stays neutral with regard to jurisdictional claims in published maps and institutional affiliations.



Copyright: © 2022 by the authors. Licensee MDPI, Basel, Switzerland. This article is an open access article distributed under the terms and conditions of the Creative Commons Attribution (CC BY) license (<https://creativecommons.org/licenses/by/4.0/>).

1. Introduction

Over the past few years, special attention has been paid to the search for new types of compounds and compositions for the creation of fuel elements with dispersed nuclear fuel, as well as materials for inert nuclear fuel matrices. Interest in these types of research is due to the need to increase the level of safety of nuclear reactors, the transition to uranium-free fuel and a decrease in the concentration of accumulated plutonium and nuclear waste [1–3]. The search for new types of materials is also due to the need to operate these materials under conditions of increased temperatures (more than 700 °C) and an increased radiation background, including neutron radiation, which initiates transmutation reactions, the product of which is the accumulation of helium, as well as interaction with fission fragments [4,5]. A distinctive feature of new types of inert matrix materials is the possibility of their operation at high temperatures due to the use of refractory oxide ceramics in them, as well as increased radiation resistance, which allows them to be operated much longer than conventional materials.

In this regard, for inert matrices of dispersed nuclear fuel in particular ceramics, the following requirements are put forward, which they must meet [6–10]. First, the inert matrix material should have good mechanical properties such as hardness, crack resistance

and strength. At the same time, these materials must not only withstand short-term effects but also maintain stability for a long time of operation and, as a result, withstand the mechanical impact of the pressure of gaseous fission products, as well as the consequences of transmutation effects. Second, the material must be stable to phase changes capable of occurring as a result of prolonged radiation exposure or thermal conductivity. Additionally, the material must be highly compatible with the fuel composition, heat transfer agent and containment material. Thirdly, the material should have high thermal conductivity and low thermal expansion coefficients, which should ensure a good transfer of thermal energy from the fuel to the coolant.

Oxide ceramics such as ZrO_2 , CeO_2 , MgO , Al_2O_3 and Y_2O_3 [11–15], as well as various more complex oxide systems, are considered some of the promising material candidates for inert matrices of dispersed nuclear fuel [11–15]. Interest in them is due to the fact that the most studied nuclear fuels are UO_2 and PuO_2 oxide fuel, as well as their physicochemical, structural and mechanical properties and small sections of thermal neutron capture. Among the variety of oxide ceramics, great interest is shown in zirconium dioxide (ZrO_2), the distinctive features of which are high chemical stability, mechanical and strength properties, as well as high compatibility, both with heat carriers and materials of fuel element shells [16,17]. However, despite the great prospects for the use of ZrO_2 ceramics, there is one significant drawback, which lies in polymorphic phase transformations resulting both from elevated temperatures and from irradiation [18,19]. To eliminate this drawback, as a rule, various dopants are used, the addition of which leads to an increase in stability for polymorphic transformations as well as an increase in the strength and mechanical properties [20]. Another promising material among oxides is CeO_2 , which has high thermal and radiation stability as well as a number of properties that allow its use not only as inert matrices but also as a solid-fuel oxide element or catalyst [21–23].

One of the areas of research in the field of searching for and studying the properties of new types of materials based on oxide matrices is the creation of composite structures having several types of phases—the so-called cermets—which have a set of properties of components used in their production as well as increased resistance to external influences [24–30].

Based on the foregoing, the purpose of this work is to obtain ZrO_2 — CeO_2 ceramics doped with yttrium of a complex multiphase composition with the formation of interstitial or substitutional solid solutions. The choice of zirconium and cerium oxides as components of the composite ceramics is due to their properties, which together should give a unique combination. The choice of yttrium as a dopant is due to the fact that, as a rule, yttrium is added to increase resistance to external influences, as well as to strengthen materials [31–33].

2. Experimental Part

The synthesis of ZrO_2 — CeO_2 ceramics was carried out using solid-phase mechanochemical synthesis followed by thermal sintering of the obtained mixtures. ZrO_2 and CeO_2 powders in equal mole fractions (0.5:0.5) were chosen as initial components for synthesis. Doping was carried out by adding $Y(NO_3)_3 \cdot 6H_2O$ at concentrations of 0.10, 0.15, 0.20 and 0.25 mol. All powders used were purchased from Sigma Aldrich (St. Louis, MO, USA), with a chemical purity of 99.95%. Thermal sintering was carried out in an SNOL muffle furnace at a temperature of 1100 °C for 5 h at a furnace heating rate of 20 °C/min, followed by cooling for 24 h together with the furnace.

For the synthesis of ceramics, a PULVERISETTE 6 planetary mill (Fritsch International, Idar-Oberstein, Germany) was used. For grinding, a tungsten carbide beaker was used, and grinding was carried out at a speed of 400 rpm for 1 h. Analysis of the mixtures obtained after mechanochemical grinding showed the absence of any impurities associated with the chipping of the balls. This was due to the fact that tungsten carbide cups and balls were used for grinding, which have excellent strength indicators.

The determination of the morphological features of the synthesized structures, depending on the concentration of the dopant, was carried out by analyzing SEM images obtained using a Jeol 7500F (Jeol, Tokyo, Japan) scanning electron microscope.

The determination of the phase composition of the synthesized ceramics, as well as the structural parameters for each phase, was carried out by full-profile analysis using the Rietveld method of X-ray diffraction patterns obtained using a D8 Advance ECO X-ray diffractometer (Bruker GmbH, Mannheim, Germany). X-ray diffraction patterns were taken in the Bragg-Brentano geometry in the angular range $2\theta = 20\text{--}90^\circ$, with a step of 0.03° . Phase refinement was carried out in the TOPAS program code using the PDF-2 (2016) database.

The mechanical properties were determined using the indentation method. The measurements were carried out on a LECO LM700 (Leco Corporation, St. Joseph, MI, USA) microhardness tester. A Vickers diamond pyramid was used as an indenter, and the load on the indenter was 50 N.

The determination of the thermal characteristics of the studied ceramics was carried out using the standard method for determining the longitudinal heat flux, the implementation of which was carried out on a KIT-800 (Moscow, Russia) device. To determine the thermal conductivity coefficient (λ , W/(m·K)), Equation (1) was used:

$$\lambda = \frac{q\delta}{t_{c1} - t_{c2}}, \quad (1)$$

where q is the heat flux density (W/m²), t_{c1} and t_{c2} are the temperatures on both sides of the sample (K) and δ is the thickness of the sample (m). The thermal conductivity was measured by the absolute stationary method of longitudinal heat flux. The sample cross-section was 5 mm × 5 mm, and the distance between the temperature sensors was 10 mm.

3. Results and Discussion

Figure 1 shows the results of the morphological changes in the synthesized ceramics, depending on the dopant concentration. In the case of the undoped ceramics, the particle shape was cubic or diamond-shaped grains, the size of which varied from 50 nm to several hundred nanometers. At the same time, most of the grains were agglomerates consisting of 5–10 grains stuck together. In the case of the doped ceramics, there were clear changes in the morphology and particle size, and the changes were directly dependent on the concentration of the dopant. At a dopant concentration of 0.10 mol, the structure exhibited small spherical grains, which were combined with larger grains to form agglomerates. At a dopant concentration of 0.15 mol, large grains were practically not observed, and the particles were porous formations of small grains. In the case of an increase in the dopant concentration to 0.20–0.25 mol, compaction of the agglomerates was observed, and at a concentration of 0.25 mol, the structure was dense agglomerates without visible cavities between the grains. This behavior may have been due to a change in the phase composition of the ceramics, depending on the dopant concentration, which led to a change in the nucleation processes upon annealing.

Figure 2 shows the X-ray diffraction patterns obtained for a series of samples with different concentrations of yttrium dopant. A common observation for all the obtained diffraction patterns is that the shape and intensity of the reflections, as well as the ratio of the reflection areas to the background area, allowed us to conclude that the synthesized ceramics obtained by thermal sintering had a high structural ordering degree. At the same time, the main change in the X-ray diffraction patterns, depending on the dopant concentration, was the shift in reflections relative to the reference lines of the corresponding phases, determined using the full-profile analysis method. Such changes due to the substitution effect with an increasing dopant concentration could be due to both structural distortions and the formation of intercalation or replacement phases. These two factors

were taken into account in the analysis and determination of the phase composition of the synthesized ceramics.

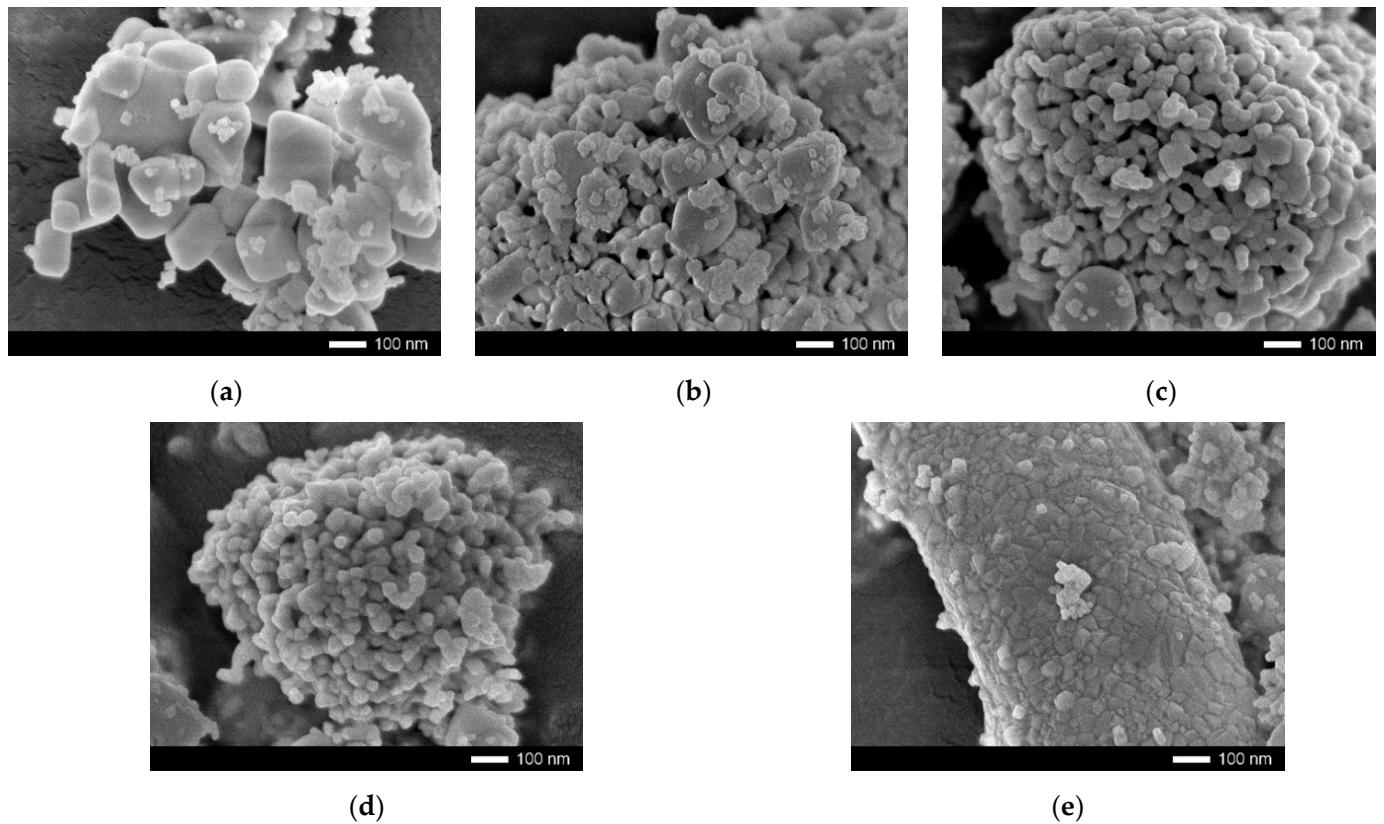


Figure 1. SEM images of morphological features of ZrO_2 — CeO_2 ceramics, depending on the concentration of the yttrium dopant: (a) 0.00 mol, (b) 0.10 mol, (c) 0.15 mol, (d) 0.20 mol and (e) 0.25 mol.

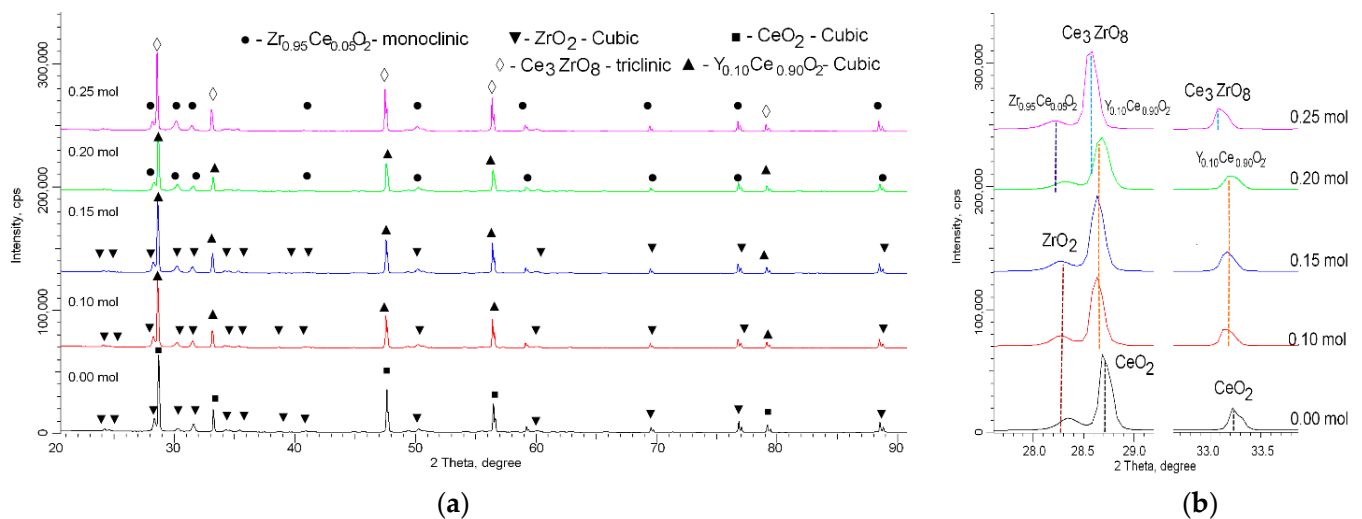


Figure 2. (a) X-ray diffraction patterns of the studied samples, depending on the dopant concentration. (b) Detailed representation of change in the position of diffraction reflections when determining the phase composition.

Figure 3 shows the phase diagram of the studied ceramics, depending on the dopant concentration. The phase composition was determined by comparing the diffraction reflection maxima with the reference values of the oxide phases characteristic of the selected components from the PDF-2(2016) database. The different phase contributions were determined using Equation (2):

$$V_{admixture} = \frac{RI_{phase}}{I_{admixture} + RI_{phase}}, \quad (2)$$

where I_{phase} is the integral intensity of the main phase of the diffraction line, $I_{admixture}$ is the average integrated intensity of the additional phase and R is the structural coefficient, which is equal to 1.45.

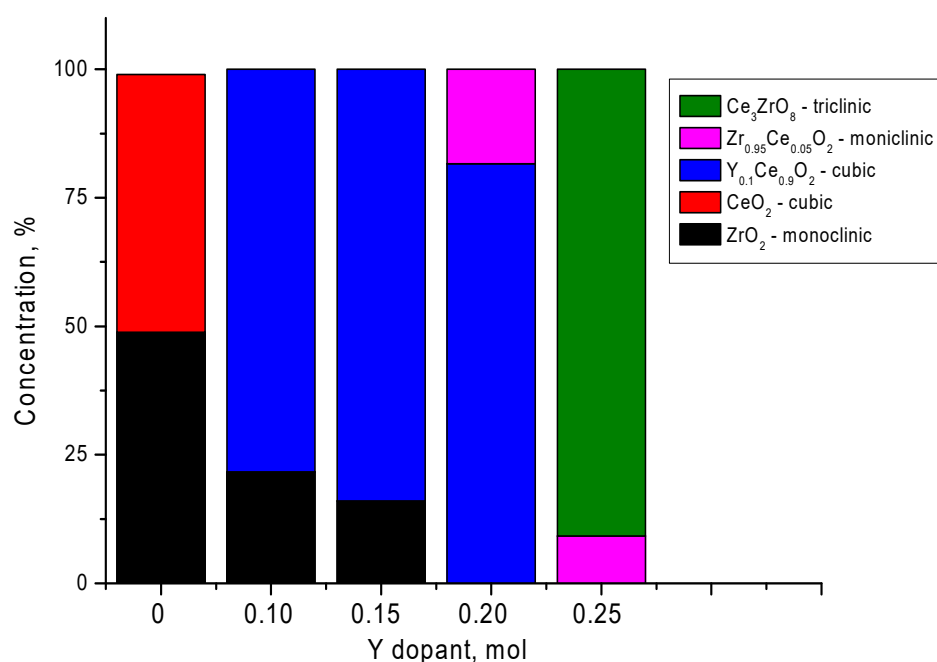


Figure 3. Diagram of the phase composition of ZrO₂—CeO₂ ceramics, depending on the yttrium dopant concentration.

The comparison took into account the effects of displacement associated with the deformation of the structure as a result of mechanochemical synthesis, as well as the possibility of the formation of interstitial phases or partial replacement. The determination of the weight contributions of various elements was determined by calculating the areas of the reflections characteristic of each phase, followed by determining the ratios of the contributions of each phase relative to all phases.

In the initial state (without the addition of a dopant), ceramics are a mixture of two phases: ZrO₂—monoclinic, $P2_1/a$ (14) (PDF-00-065-0728) and CeO₂—Cubic, $Fm\bar{3}m$ (225) (PDF-01-075-0174). The ratio of the contributions of these phases was ZrO₂:CeO₂ → 49/51, which was close to the equilibrium stoichiometry of the composition. A mixture of two phases is typical for the formation of a substitutional solid solution. An analysis of the crystal lattice parameters presented in Table 1 indicates the presence of lattice deformation for both phases, which could be due to both mechanochemical synthesis and the process of the substitution of atoms in both types of crystal lattices.

Table 1. Data of the crystal lattice parameters of the studied ceramics.

Parameter	Y Dopant (mol)				
	0	0.10	0.15	0.20	0.25
ZrO ₂ –monoclinic, <i>P2₁/a</i> 14	a = 5.2961 ± 0.0013 Å, b = 5.1896 ± 0.0015 Å, c = 5.1238 ± 0.0012 Å, β = 99.056°, V = 139.07 Å ³	a = 5.3129 ± 0.0017 Å, b = 5.1907 ± 0.0012 Å, c = 5.1229 ± 0.0015 Å, β = 99.135°, V = 139.49 Å ³	a = 5.3172 ± 0.0015 Å, b = 5.1876 ± 0.0012 Å, c = 5.1380 ± 0.0016 Å, β = 99.131°, V = 139.93 Å ³	-	-
CeO ₂ –Cubic, <i>Fm$\bar{3}m$</i> (225)	a = 5.3851 ± 0.0016 Å, V = 156.16 Å ³	-	-	-	-
Y _{0.1} Ce _{0.9} O ₂ –Cubic, <i>Fm$\bar{3}m$</i> (225)	-	a = 5.3966 ± 0.0021 Å, V = 157.17 Å ³	a = 5.3945 ± 0.0019 Å, V = 156.98 Å ³	a = 5.3873 ± 0.0009 Å, V = 156.35 Å ³	-
Zr _{0.95} Ce _{0.05} O ₂ –monoclinic, <i>P2₁/a</i> 14	-	-	-	a = 5.3136 ± 0.0011 Å, b = 5.1828 ± 0.0009 Å, c = 5.3081 ± 0.0015 Å, β = 99.158°, V = 138.88 Å ³	a = 5.3308 ± 0.0014 Å, b = 5.1886 ± 0.0016 Å, c = 5.1531 ± 0.0012 Å, β = 99.310°, V = 140.65 Å ³
Ce ₃ ZrO ₈ –triclinic, <i>P1</i> (1)	-	-	-	-	a = 7.6343 ± 0.0019 Å, b = 7.6313 ± 0.0012 Å, c = 5.4209 ± 0.0014 Å, α = 89.841°, β = 89.771°, γ = 90.299°, V = 315.81 Å ³

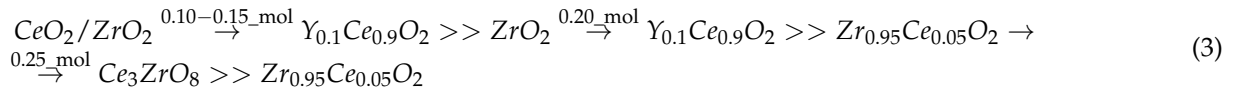
For samples with a dopant concentration of 0.10 mol, the shift of the main reflections for the previously observed CeO₂ phase (initial sample) corresponded to the position of the reflections characteristic of the Y_{0.1}Ce_{0.9}O₂–Cubic, *Fm $\bar{3}m$* (225) cubic phase, which indicates that when the dopant was added, the formation of a phase of partial replacement of cerium atoms by yttrium dopant atoms at the sites of the crystal lattice occurred. At the same time, the analysis of changes in the crystal lattice parameters for the ZrO₂ phase indicates that their increase could also be due to the partial replacement of zirconium atoms by yttrium atoms but without the formation of a full-weight substitution phase, as in the case of the CeO₂ phase. This assumption is based on the difference in the atomic radii of zirconium (0.140–0.160 nm) and yttrium (0.180 nm). At the same time, the analysis of the contributions of various phases indicates the dominance of the Y_{0.1}Ce_{0.9}O₂ phase in the structure of the ceramics.

A similar situation was observed for the samples with a dopant concentration of 0.15 mol, for which the main structural changes were associated with a change in the crystal lattice parameters, as well as a slight increase in the contribution of the Y_{0.1}Ce_{0.9}O₂ phase.

A new type of structural and phase changes was observed with an increase in the dopant concentration from 0.15 to 0.20, which was associated with the displacement of the ZrO₂ phase from the ceramic composition and the formation of a new Zr_{0.95}Ce_{0.05}O₂–monoclinic, *P2₁/a* 14 substitution phase. The formation of this phase may have been due to recrystallization processes caused by a high content of the dopant, as well as partial replacement of zirconium atoms by cerium atoms, which were displaced from the Y_{0.1}Ce_{0.9}O₂ phase as a result of the substitution of yttrium for cerium.

A further increase in the dopant concentration to 0.25 mol led to the formation of the Ce₃ZrO₈–triclinic *P1* (1) phase, with parameters characteristic of the substitution phase, the increase in which may have been due to the partial replacement of cerium or zirconium atoms by yttrium atoms.

Based on the phase composition analysis, it was possible to compile a characteristic phase diagram of transformations depending on the concentration of the dopant, which could be written as the following expression (3):



Thus, by analyzing the obtained data on changes in the phase composition, depending on the dopant concentration, it could be concluded that by using this synthesis method under given conditions and certain dopant concentrations, it is possible to obtain ceramics with a complex two-phase composition similar to substitutional phases.

An important factor in evaluating the ceramic properties is the study of their strength properties, the determination of which makes it possible to evaluate the resistance of ceramics to external influences as well as determine their resistance to mechanical influences. Figure 4 shows the results of determining the microhardness of the synthesized ceramics, depending on the dopant concentration. The measurement error was determined by measuring 25–30 consecutive indentations and determining the mean value and standard deviation.

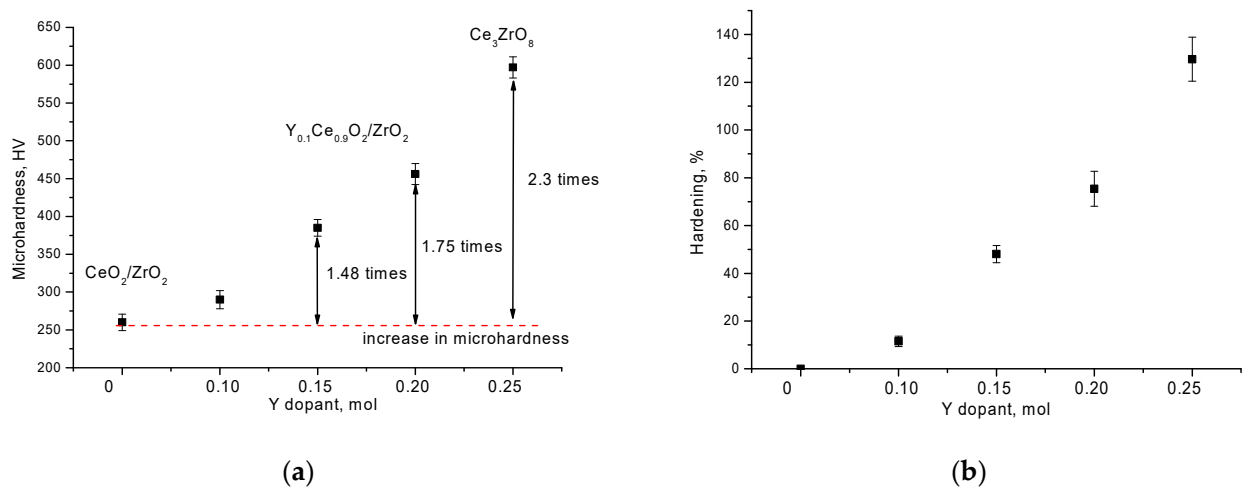


Figure 4. (a) The results of changing the value of the microhardness depending on the dopant concentration. (b) Results of ceramic hardening, depending on dopant concentration.

As can be seen from the data presented, the addition of a dopant, which led to a change in the morphological features of the ceramics, led to an increase in the microhardness and strengthening of the ceramics to external influences (see the results in Figure 4b). At the same time, the formation of the $\text{Y}_{0.1}\text{Ce}_{0.9}\text{O}_2$ phase in the structure led to an increase in hardness by factors of 1.5 and 1.75, which indicates a high resistance to external influences. The dominance of the Ce_3ZrO_8 phase in the structure and the formation of dense ceramics led to strengthening of the ceramics by more than two times. Such behavior of the mechanical properties and an increase in hardness indicate an increase in resistance to the formation of microcracks and deformation of the structure, which may have been due to the effect associated with a change in the dislocation density in the structure, as well as phase formation processes, with a change in dopant concentration. The change in the dislocation density could be estimated by analyzing the sizes of the crystallites obtained from the X-ray diffraction data using the following standard formula (4):

$$\delta = \frac{1}{L^2} \quad (4)$$

where L is the crystallite size. The calculation results are shown in Figure 5.

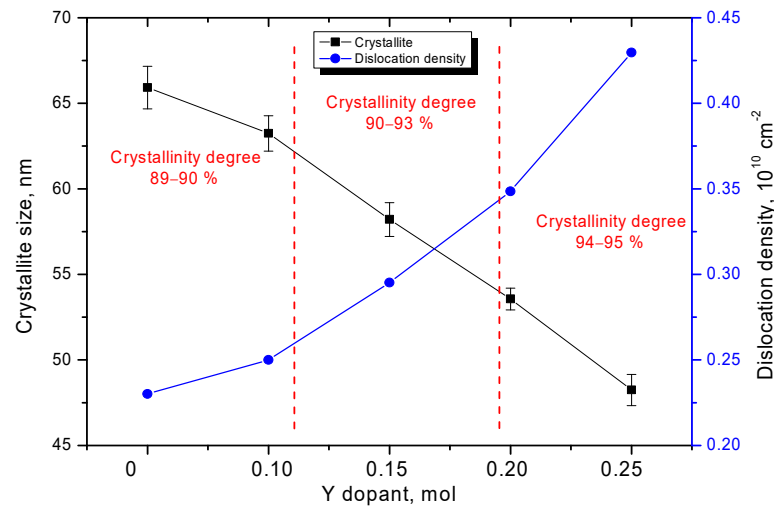


Figure 5. Results of changes in the crystallite sizes and dislocation density.

A decrease in the crystallite size depending on the change in phase composition led to an increase in the dislocation density, a change which, as is known, can have a strengthening effect on the formation of microcracks and cleavages as a result of deformation and also affect the increase in crack resistance [34,35]. At the same time, it can be seen that the increase in dislocation density had a similar dependence with the results of hardening of ceramics. Thus, we can conclude that the hardening effect was associated with a change in the dislocation density and an increase in the structural ordering degree. The structural ordering degree (crystallinity degree) was estimated by comparing the areas of reflections and background radiation characteristics of the amorphous or disordered inclusions in the structure. The crystallinity degree was determined by approximating the diffraction spectra with the necessary number of pseudo-Voigt functions and then comparing the areas of the diffraction reflections and the background line, which are characteristic of disordered inclusions.

One of the important characteristics of inert matrix materials is thermal conductivity, which reflects the interaction of the ceramics of the inert matrix with the fuel element wall material or coolant during heat transfer during operation. The results are shown in Figure 6.

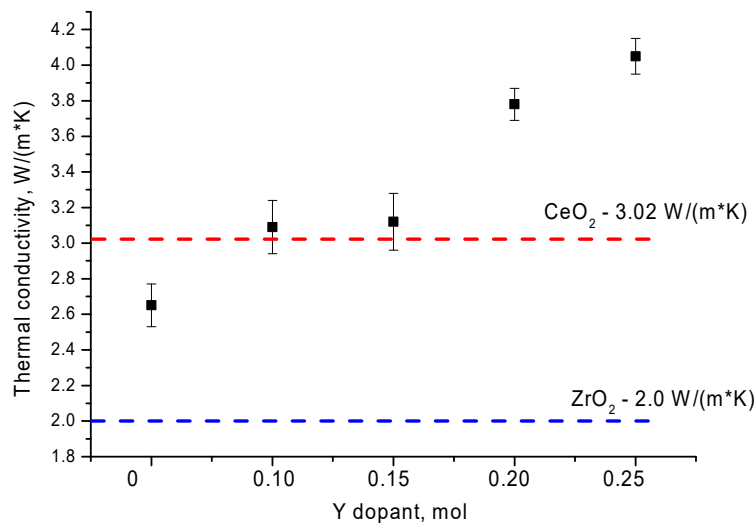


Figure 6. The results of the change in the thermal conductivity coefficient (dotted lines indicate the thermal conductivity coefficient values for ZrO_2 and CeO_2).

As can be seen from the presented data, in the case of mixing two components and obtaining a structure similar to the solid solution of the ZrO_2 and CeO_2 phases, the value of the thermal conductivity coefficient was greater than that for pure ZrO_2 and less than that for CeO_2 , which indicates that in the formation of heat-conducting properties, the dominant role was played by cerium oxide. In the case of doping, the value of the thermal conductivity increased, which indicates a positive effect of the formation of two-phase structures containing yttrium on the heat-conducting properties. In the case where the structure was dominated by the Ce_3ZrO_8 phase, the thermal conductivity coefficient increased by a factor of 1.5 compared with the ceramics in the form of a solid solution of the ZrO_2 and CeO_2 phases.

4. Conclusions

This work is devoted to the study of the structural, strength and heat-conducting properties of ZrO_2 — CeO_2 ceramics doped with yttrium, obtained by mechanochemical solid-phase synthesis. During the analysis of the obtained X-ray diffraction patterns, it was found that by using this synthesis method under given conditions and certain dopant concentrations, it was possible to obtain ceramics with a complex two-phase composition of the type of substitution phases. It was determined that an increase in the dopant concentration, which led to a change in the phase composition of the ceramics, led to an increase in the mechanical strength and thermal conductivity of the ceramics. The main mechanism for changing the strength properties was a change in the dislocation density of the ceramics as a result of recrystallization and phase transformations.

Further research will be aimed at studying the resistance of synthesized ceramics to external influences, including the processes of gaseous swelling under irradiation with heavy ions and helium ions, comparable to the effects that arise during the operation of materials in a nuclear reactor.

Author Contributions: Conceptualization, D.I.S., S.G.G., N.A.S., E.N., M.V.Z. and A.L.K.; methodology, D.I.S., S.G.G., N.A.S., E.N., M.V.Z. and A.L.K.; formal analysis, D.I.S., S.G.G., N.A.S., E.N., M.V.Z. and A.L.K.; investigation, D.I.S., S.G.G., N.A.S., E.N., M.V.Z. and A.L.K.; resources, A.L.K.; writing—original draft preparation, review and editing, D.I.S. and A.L.K.; visualization, A.L.K.; supervision, A.L.K. All authors have read and agreed to the published version of the manuscript.

Funding: This research was funded by the Science Committee of the Ministry of Education and Science of the Republic of Kazakhstan (No. BR11765580).

Institutional Review Board Statement: Not applicable.

Informed Consent Statement: Not applicable.

Data Availability Statement: Not applicable.

Conflicts of Interest: The authors declare that they have no conflict of interest.

References

1. Lombardi, C.; Luzzi, L.; Padovani, E.; Vettriano, F. Thoria and inert matrix fuels for a sustainable nuclear power. *Prog. Nucl. Energy* **2008**, *50*, 944–953. [[CrossRef](#)]
2. Ledergerber, G.; Deguelde, C.; Heimgartner, P.; Pouchon, M.; Kasemeyer, U. Inert matrix fuel for the utilisation of plutonium. *Prog. Nucl. Energy* **2001**, *38*, 301–308. [[CrossRef](#)]
3. Nandi, C.; Grover, V.; Bhandari, K.; Bhattacharya, S.; Mishra, S.; Banerjee, J.; Prakash, A.; Tyagi, A. Exploring YSZ/ ZrO_2 — PuO_2 systems: Candidates for inert matrix fuel. *J. Nucl. Mater.* **2018**, *508*, 82–91. [[CrossRef](#)]
4. Golovkina, L.S.; Orlova, A.I.; Nokhrin, A.V.; Boldin, M.S.; Lantsev, E.A.; Chuvil'deev, V.N.; Sakharov, N.V.; Shotin, S.V.; Zelenov, A.Y. Spark Plasma Sintering of fine-grained ceramic-metal composites YAG: Nd-(W, Mo) based on garnet-type oxide $Y_{2.5}Nd_{0.5}Al_5O_{12}$ for inert matrix fuel. *J. Nucl. Mater.* **2018**, *511*, 109–121. [[CrossRef](#)]
5. Ang, C.; Snead, L.; Kato, Y. A logical approach for zero-rupture Fully Ceramic Microencapsulated (FCM) fuels via pressure-assisted sintering route. *J. Nucl. Mater.* **2020**, *531*, 151987. [[CrossRef](#)]
6. Savchyn, V.P.; Popov, A.I.; Aksimentyeva, O.I.; Klym, H.; Horbenko, Y.Y.; Serga, V.; Moskina, A.; Karbovnyk, I. Cathodoluminescence characterization of polystyrene-BaZrO₃ hybrid composites. *Low Temp. Phys.* **2016**, *42*, 597–600. [[CrossRef](#)]

7. Van Vuuren, A.J.; Skuratov, V.; Ibrayeva, A.; Zdorovets, M. Microstructural Effects of Al Doping on Si₃N₄ Irradiated with Swift Heavy Ions. *Acta Phys. Pol. A* **2019**, *136*, 241–244. [[CrossRef](#)]
8. Settar, A.; Abboudi, S.; Lebaal, N. Effect of inert metal foam matrices on hydrogen production intensification of methane steam reforming process in wall-coated reformer. *Int. J. Hydrogen Energy* **2018**, *43*, 12386–12397. [[CrossRef](#)]
9. Manara, D.; Najj, M.; Mastromarino, S.; Elorrieta, J.; Magnani, N.; Martel, L.; Colle, J.-Y. The Raman fingerprint of plutonium dioxide: Some example applications for the detection of PuO₂ in host matrices. *J. Nucl. Mater.* **2018**, *499*, 268–271. [[CrossRef](#)]
10. Mikhailov, D.A.; Orlova, A.I.; Malanina, N.V.; Nokhrin, A.V.; Potanina, E.A.; Chuvil'deev, V.N.; Boldin, M.S.; Sakharov, N.V.; Belkin, O.A.; Kalenova, M.Y.; et al. A study of fine-grained ceramics based on complex oxides ZrO₂-Ln₂O₃ (Ln = Sm, Yb) obtained by Spark Plasma Sintering for inert matrix fuel. *Ceram. Int.* **2018**, *44*, 18595–18608. [[CrossRef](#)]
11. Monge, M.A.; González, R.; Muñoz-Santiuste, J.E.; Pareja, R.; Chen, Y.; Kotomin, E.A.; Popov, A.I. Photoconversion and dynamic hole recycling process in anion vacancies in neutron-irradiated MgO crystals. *Phys. Rev. B* **1999**, *60*, 3787–3791. [[CrossRef](#)]
12. Monge, M.A.; González, R.; Muñoz-Santiuste, J.E.; Pareja, R.; Chen, Y.; Kotomin, E.; Popov, A. Photoconversion of F⁺ centers in neutron-irradiated MgO. *Nucl. Instrum. Methods Phys. Res. Sect. B Beam Interact. Mater. At.* **2000**, *166*, 220–224. [[CrossRef](#)]
13. Kadyrzhanov, K.K.; Tinishbaeva, K.; Uglov, V.V. Investigation of the effect of exposure to heavy Xe²²⁺ ions on the mechanical properties of carbide ceramics. *Eurasian Phys. Tech. J.* **2021**, *17*, 46–53. [[CrossRef](#)]
14. Popov, A.; Lushchik, A.; Shablonin, E.; Vasil'Chenko, E.; Kotomin, E.; Moskina, A.; Kuzovkov, V. Comparison of the F-type center thermal annealing in heavy-ion and neutron irradiated Al₂O₃ single crystals. *Nucl. Instrum. Methods Phys. Res. Sect. B Beam Interact. Mater. At.* **2018**, *433*, 93–97. [[CrossRef](#)]
15. Degueldre, C.; Hellwig, C. Study of a zirconia based inert matrix fuel under irradiation. *J. Nucl. Mater.* **2003**, *320*, 96–105. [[CrossRef](#)]
16. Chauvin, N.; Konings, R.; Matzke, H. Optimisation of inert matrix fuel concepts for americium transmutation. *J. Nucl. Mater.* **1999**, *274*, 105–111. [[CrossRef](#)]
17. Vu, T.M.; Hartanto, D.; Chu, T.N.; Pham, N.V.H.; Bui, T.H. Sensitivity and uncertainty analysis of neutronic and kinetic parameters for CERCER and CERMET fueled ADS using SERPENT 2 and ENDF/B-VIII.0. *Ann. Nucl. Energy* **2021**, *168*, 108912. [[CrossRef](#)]
18. Costa, D.R.; Liu, H.; Lopes, D.A.; Middleburgh, S.C.; Wallenius, J.; Olsson, P. Interface interactions in UN-X-UO₂ systems (X = V, Nb, Ta, Cr, Mo, W) by pressure-assisted diffusion experiments at 1773 K. *J. Nucl. Mater.* **2022**, *561*, 153554. [[CrossRef](#)]
19. Alin, M.; Kozlovskiy, A.L.; Zdorovets, M.V.; Uglov, V.V. Study of the mechanisms of the t-ZrO₂ → c-ZrO₂ type polymorphic transformations in ceramics as a result of irradiation with heavy Xe²²⁺ ions. *Solid State Sci.* **2022**, *123*, 106791. [[CrossRef](#)]
20. Ivanov, I.A.; Alin, M.; Koloberdin, M.V.; Sapar, A.; Kurakhmedov, A.E.; Kozlovskiy, A.L.; Zdorovets, M.V.; Uglov, V.V. Effect of irradiation with heavy Xe²²⁺ ions with energies of 165–230 MeV on change in optical characteristics of ZrO₂ ceramic. *Opt. Mater.* **2021**, *120*, 111479. [[CrossRef](#)]
21. Zhang, Y.; Chen, H.X.; Duan, L.; Fan, J.B.; Ni, L.; Ji, V. A comparison study of the structural and mechanical properties of cubic, tetragonal, monoclinic, and three orthorhombic phases of ZrO₂. *J. Alloys Compd.* **2018**, *749*, 283–292. [[CrossRef](#)]
22. Aksimentyeva, O.I.; Savchyn, V.P.; Dyakonov, V.P.; Piechota, S.; Horbenko, Y.Y.; Opainych, I.Y.; Demchenko, P.Y.; Popov, A.; Szymczak, H. Modification of Polymer-Magnetic Nanoparticles by Luminescent and Conducting Substances. *Mol. Cryst. Liq. Cryst.* **2014**, *590*, 35–42. [[CrossRef](#)]
23. Kim, S.-E.; Yoon, J.-K.; Shon, I.-J. Mechanochemical Synthesis and Rapid Consolidation of Nanostructured Nb-ZrO₂ Composite. *J. Nanosci. Nanotechnol.* **2020**, *20*, 4253–4256. [[CrossRef](#)] [[PubMed](#)]
24. Shelyug, A.; Navrotsky, A. Thermodynamic stability of the fluorite phase in the CeO₂–CaO–ZrO₂ system. *J. Nucl. Mater.* **2019**, *517*, 80–85. [[CrossRef](#)]
25. Kumar, R.; Chauhan, V.; Gupta, D.; Upadhyay, S.; Ram, J.; Kumar, S. Advancement of High-k ZrO₂ for Potential Applications: A Review. *Indian J. Pure Appl. Phys. (IJPAP)* **2021**, *59*, 811–826.
26. Alekseeva, L.S.; Nokhrin, A.V.; Boldin, M.S.; Lantsev, E.A.; Orlova, A.I.; Chuvil'Deev, V.N.; Sakharov, N.V. Preparation of Fine-Grained CeO₂-SiC Ceramics for Inert Fuel Matrices by Spark Plasma Sintering. *Inorg. Mater.* **2020**, *56*, 1307–1313. [[CrossRef](#)]
27. Hudák, I.; Skryja, P.; Bojanovský, J.; Jegla, Z.; Krňávek, M. The Effect of Inert Fuel Compounds on Flame Characteristics. *Energies* **2021**, *15*, 262. [[CrossRef](#)]
28. Mareš, K.V.; John, J. Recycling of isotopically modified molybdenum from irradiated CerMet nuclear fuel: Part 1—concept design and assessment. *J. Radioanal. Nucl. Chem.* **2019**, *320*, 227–233. [[CrossRef](#)]
29. Baron, R.; Wejrzanowski, T.; Milewski, J.; Szablowski, L.; Szczeńniak, A.; Fung, K.-Z. Manufacturing of γ-LiAlO₂ matrix for molten carbonate fuel cell by high-energy milling. *Int. J. Hydrogen Energy* **2018**, *43*, 6696–6700. [[CrossRef](#)]
30. Sharma, S.K.; Grover, V.; Tyagi, A.; Avasthi, D.; Singh, U.; Kulriya, P. Probing the temperature effects in the radiation stability of Nd₂Zr₂O₇ pyrochlore under swift ion irradiation. *Materialia* **2019**, *6*, 100317. [[CrossRef](#)]
31. Mistarihi, Q.M.; Park, W.; Nam, K.; Yahya, M.-S.; Kim, Y.; Ryu, H.J. Fabrication of oxide pellets containing lumped Gd₂O₃ using Y₂O₃-stabilized ZrO₂ for burnable absorber fuel applications. *Int. J. Energy Res.* **2018**, *42*, 2141–2151. [[CrossRef](#)]
32. Wen, T.; Yuan, L.; Tian, C.; Yan, Z.; Liu, Z.; Yu, J. Electrical conductivity behavior of ZrO₂-MgO-Y₂O₃ ceramic: Effect of heat treatment temperature. *J. Aust. Ceram. Soc.* **2022**, 1–7. [[CrossRef](#)]

33. Marek, I.O.; Dudnik, O.V.; Korniy, S.A.; Red'ko, V.P.; Danilenko, M.I.; Ruban, O.K. Effect of Heat Treatment in the Temperature Range 400–1300 °C on the Properties of Nanocrystalline ZrO₂– Y₂O₃– CeO₂ Powders. *Powder Metall. Met. Ceram.* **2022**, *60*, 1–11. [[CrossRef](#)]
34. Dehm, G.; Jaya, B.; Raghavan, R.; Kirchlechner, C. Overview on micro- and nanomechanical testing: New insights in interface plasticity and fracture at small length scales. *Acta Mater.* **2018**, *142*, 248–282. [[CrossRef](#)]
35. Nykyforchyn, H.; Kyryliv, V.; Maksymiv, O.; Zvirko, O. Mechanical fabrication methods of nanostructured surfaces. In *Handbook of Modern Coating Technologies*; Elsevier: Amsterdam, The Netherlands, 2021; pp. 25–67.